Performance of the newly installed vertical neutron cameras for low neutron yield discharges in the Large Helical Device

Performance of the newly installed vertical neutron cameras for low neutron yield discharges in the Large Helical Device

S. Sangaroon, K. Ogawa, M. Isobe, et al.

View Online   Export Citation   CrossMark

ARTICLES YOU MAY BE INTERESTED IN

Performance of the newly installed vertical neutron cameras for low neutron yield discharges in the Large Helical Device

S. Sangaroon,[1,a] K. Ogawa,[1,2,b] M. Isobe,[1,2,c] M. I. Kobayashi,[1,2,d] Y. Fujiwara,[1,e] S. Kamio,[1,f]
R. Seki,[1,2,g] H. Nuga,[1,h] H. Yamaguchi,[1,i] and M. Osakabe[1,2,j]

AFFILIATIONS

[1] National Institute for Fusion Science, National Institutes of Natural Sciences, Toki 509-5292, Japan
[2] The Graduate University for Advanced Studies, SOKENDAI, Toki, 509-5292, Japan

[a] Author to whom correspondence should be addressed: sangaroon.siriyaporn@nifs.ac.jp
[b] E-mail: kogawa@nifs.ac.jp
[c] E-mail: isobe@nifs.ac.jp
[d] E-mail: kobayashi.makoto@nifs.ac.jp
[e] E-mail: fujiwara.yutaka@nifs.ac.jp
[f] E-mail: kamio@nifs.ac.jp
[g] E-mail: seki.ryohsuke@nifs.ac.jp
[h] E-mail: nuga.hideo@nifs.ac.jp
[i] E-mail: yamaguchi.hiroyuki@nifs.ac.jp
[j] E-mail: osa@nifs.ac.jp

ABSTRACT

Two new vertical neutron cameras characterized by high detection efficiency were developed on the Large Helical Device in order to observe poloidal structures of helically trapped beam ions created by the perpendicularly injected positive-ion based neutral beam (P-NB) and are newly operated since 2018. In this work, the neutron fields at the vertical neutron cameras are investigated using the Monte Carlo N-particle transport code to evaluate the performance of its collimators. The results indicate that neutrons are attenuated by the heavy concrete and are well collimated through the collimator to detectors. Neutron spectra at the detector position show over 99% of uncollided 2.45 MeV neutrons. Time evolution of neutron emission profiles during the short pulse of P-NB injection is measured by the vertical neutron cameras. Peaks on the neutron emission profiles corresponding to the helically trapped beam ion are successfully obtained, as designed. The decrease in line integrated neutron flux at the peak positions after the P-NB stops is consistent with the behavior of the total neutron emission rate measured by the neutron flux monitor.

Published under license by AIP Publishing. https://doi.org/10.1063/5.0010302

I. INTRODUCTION

Understanding of energetic particle transport and loss due to the energetic-particle-driven magnetohydrodynamic (MHD) mode is one of the key issues in order to obtain better plasma performance in fusion devices.[1] The energetic particle transport behaviors were successfully demonstrated in tokamaks using the neutron camera. A neutron camera based on parallel collimators was installed in the basement of the Tokamak Fusion Test Reactor (TFTR).[2,3]

The time-resolved and the spatially resolved neutron emission profiles during high frequency MHD activity were obtained in TFTR.[3] The horizontal and vertical neutron cameras were installed at the Joint European Torus (JET).[4,5] The instruments allow us to study the evolution of neutron emissivity poloidal distribution using the tomographic reconstruction method.[6] The vertically inclined multichannel collimator was installed at the JAERI Tokamak 60 Upgrade (JT-60U).[7,8] The energetic ion transport during the neutral beam heating is observed with the neutron camera at JT-60U.[9]

The horizontal and vertical neutron cameras based on the JET neutron camera is planned to be installed at ITER.[10,11] The understanding of energetic particle physics obtained by the neutron camera will provide essential information for the achievement of burning plasma in ITER.

In stellarators and helical devices, in particular, the behavior of helically trapped beam ion that is created by the perpendicularly neutral beam injections is crucial in the core plasma physics regarding the loss of the energetic ion or the limiting of the ion temperature because of a lack of symmetry of the system. The loss of helically trapped beam proton perpendicularly injected by a diagnostic neutral beam injector was investigated in the Compact Helical System (CHS) with a conventional neutral particle analyzer (NPA).[12] During the hydrogen plasma experiment of Large Helical Device (LHD), the fast ions confinements during the ion cyclotron resonance heating and neutral beam heating were experimentally investigated[13] using a comprehensive set of fast ion diagnostics.[14] In particular, confinement property of the helically trapped proton accelerated by ion cyclotron resonance heating has been studied in the LHD using the natural diamond detectors as a solid-state NPA.[15] In order to sustain the high-temperature state, the study of helically trapped beam ion behavior is important and will provide the crucial information for the deep understanding of energetic ions confinement property. Unlike the combination of a hydrogen discharge and NPA, in deuterium discharges, the information related to the energetic ions behavior in plasma core can be directly obtained from neutrons, which are mainly produced from the reaction between beam ions and bulk ions. The LHD equipped with three tangentially injected negative-ion-source-based neutral beam injections and two perpendicularly injected positive-ion-source-based neutral beam injections (P-NBs) can provide heating power up to 35 MW. The deuterium plasma experiments have been operated at LHD since March 2017. The expected maximum total neutron emission rate (S_n) is 1.9×10^{16} n/s.[16] The comprehensive neutron diagnostics are developed and working at LHD in order to enhance the understanding of the energetic-particle physics in the LHD.[17–19] To study the energetic particle transport through the time-resolved and the spatially resolved measurement, the neutron cameras have been developed and used in LHD. The first vertical neutron camera (the so-called VNC1) was developed for working at S_n of 1.9×10^{16} n/s.[20,21] VNC1 has been providing the crucial information in order to study the energetic ion confinement property in LHD.[17,18,22,23] However, in the plasma discharge with strong MHD activities, S_n is approximately two orders of magnitude lower ($S_n \sim 3 \times 10^{14}$ n/s) than the expected maximum S_n.[23] To achieve higher time-resolved neutron emission profile measurements during MHD activities, new vertical neutron cameras (the so-called VNC2 and the so-called VNC3) characterized by a high detection efficiency were developed and are operated since 2018. This paper is devoted to discussing the performance of VNC2 and VNC3 using numerical simulation and shows experimental results.

II. NEW VERTICAL NEUTRON CAMERAS

The VNC2 has nine sight lines each having an inner diameter of 5 cm. Sight lines align radially at radius (R) of 3.339 m, 3.420 m, 3.501 m, 3.644 m, 3.725 m, 3.806 m, 3.949 m, 4.021 m, and 4.093 m. The VNC3 has eight sight lines each having an inner

diameter of 5 cm. Sight lines align radially at R of 3.4 m, 3.5 m, 3.6 m, 3.7 m, 3.8 m, 3.9 m, 4.0 m, and 4.1 m. The VNC2 and VNC3 are installed parallel at the LHD lower port (the so-called 1.5L port) to view different plasma cross sections in order to observe the poloidal structure of helically trapped beam ions created by the P-NBs.[24] Figure 1(a) shows the location of the P-NB#4, P-NB#5, and two helical ripples A and B between the two helical coils. Figure 1(b) shows the horizontally elongated poloidal cross section where the P-NB is injected at the helical ripple A. As shown in Fig. 1(a), both P-NBs mainly create helically trapped beam ions in the helical ripple A. The typical density profile of beam ion created by P-NBs calculated using the guiding center orbit following model MORH code[25] together with the VNCs sight line is shown in Fig. 2. The
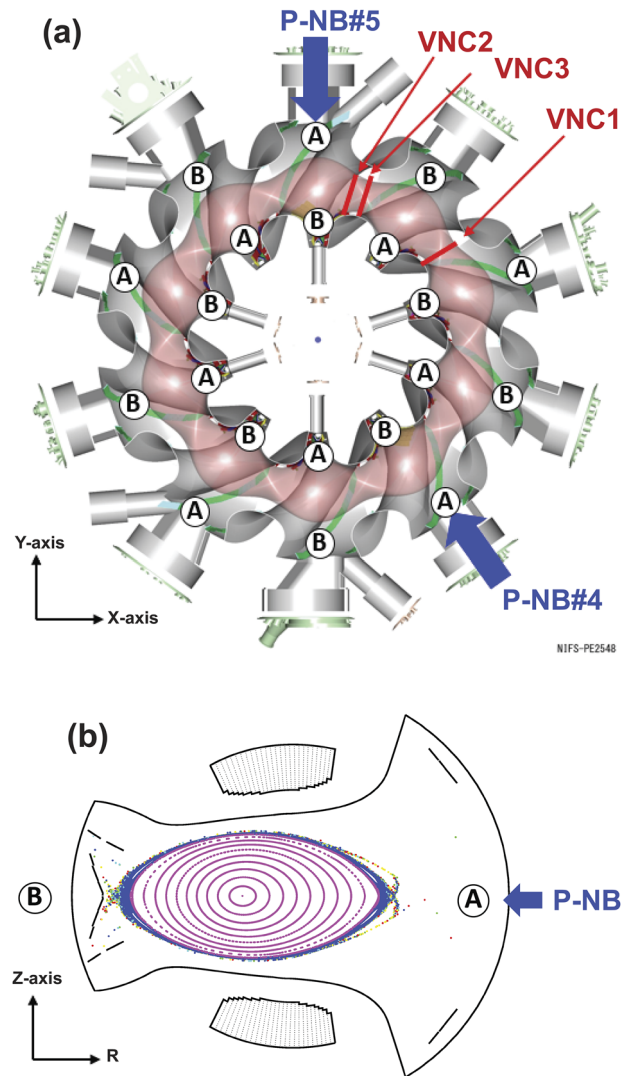

FIG. 1. (a) A schematic view of LHD and the position of P-NBs heating injections; A and B are the outer and inner helical ripple regions between the coil. The location of VNC2 and VNC3 are also shown. (b) A horizontally elongated poloidal cross section together with helical winding coil where the P-NB is injected.
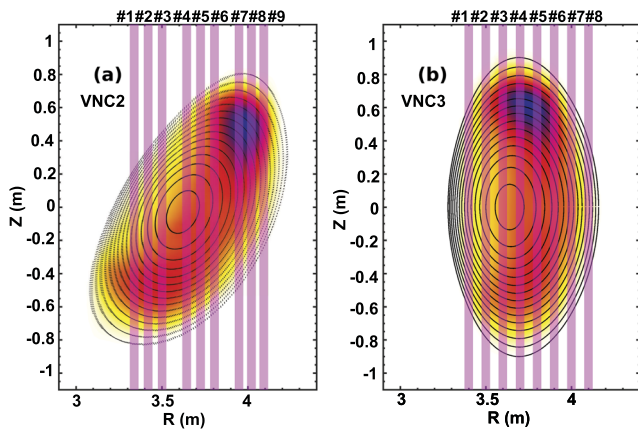
FIG. 2. Typical density profile of beam ions created by the P-NBs (a) where the VNC2 is installed and (b) where the VNC3 is installed. Vertical pink bars indicate sight lines of VNCs.

FIG. 3. MCNP calculation models of (a) VNC2 calculation and (b) VNC3 calculations.

relatively high-density region of helically trapped beam ion appears in the upper region of poloidal cross sections at VNC2 and VNC3 positions, which correspond to the helical ripple A. The detectors used in the neutron camera are model EJ-410[26] and are based on silver activated zinc sulfide phosphor (ZnS:Ag) embedded in the hydrogenous polymer matrix structured in a series of concentric cylinders with a diameter of 5.08 cm and a thickness of 1.58 cm. EJ-410 has high fast neutron detection efficiency (E_n > 1 MeV) and is insensitive to gamma rays. The EJ-410 scintillator is directly coupled with the two-inch size photomultiplier (H7195, Hamamatsu Photonics K.K.).[27] The anode signal is fed into the low-impedance current amplifier (C7319, Hamamatsu Photonics K.K.).[28] The detectors are operated with current mode to record the neutron emissivity profile with a higher temporal resolution (up to 200 kHz). The detectors are equipped to the fast digitizer acquisition system with the sampling frequency of 1 MHz (PXI6133, National Instruments).[29]

III. NEUTRONICS CALCULATION

A. Modeling for MCNP calculation

The neutron fields at VNC2 and VNC3 are investigated using the Monte Carlo N-Particle (MCNP) transport code MCNP6[30] and the cross section library of FENDL-3.0.[31] The LHD and torus hall were modeled based on the simplified computer aided design (CAD) drawing.[32–35] In this calculation, parallel vertical sight lines of stainless steel (SUS304) pipes with 5 cm inner diameter and 0.1 cm thick embedded in the 1.5 m thick hematite (Fe_2O_3)-doped heavy concrete and installed in the 2 m thick torus floor ordinary concrete are modeled as collimators at 1.5L port of LHD for VNC2 and VNC3, as shown in Figs. 3(a) and 3(b), respectively. The hematite heavy concrete used for VNC2 and VNC3 is the same as that used for VNC1,[21] which provides low level of unwanted gamma rays compared to the collimator made of polyethylene. An array of stainless steel (SUS304) pipes with an inner diameter of 3.8 cm, a length of 416 cm, and a thickness of 0.15 cm that is used for the neutral particle analyzer based on the single crystal CVD diamond detector[36] is
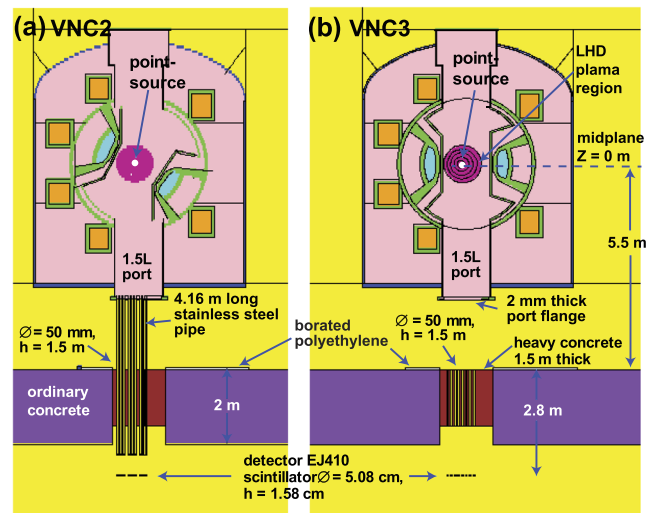
modeled along the VNC2. The 2 mm thick port flange is modeled for VNC3. To study the collimator performance and spatial resolution of the VNCs, a point neutron source with the energy of 2.45 MeV is used and located on the torus midplane (Z = 0 m) at the collimator central axis of the primary channel of VNC2 and VNC3 calculations (see the channel number in Table I). The neutron field has been calculated by using track length estimation tally (the so-called cell tally in MCNP6) with a volume of 32.18 cm³, which is located at Z = 8.3 m below the midplane. Note that the neutron flux in this work is presented in relative value.

B. Calculation results of a point neutron source

1. Neutron distribution

Figures 4(a) and 4(b) show the image plots of neutron flux distribution in energy range of 0.1 MeV–2.45 MeV at VNC2 and at VNC3 cross section, respectively. It is clearly seen that neutrons are attenuated by the heavy concrete and are well collimated through the primary collimators to the detectors. It is clearly seen in Fig. 4(b) that the neutron is observed by the neighboring channels, which is referred to as a neutron crosstalk. Here, we define the neutron crosstalk by the ratio of the average neutron flux measured at secondary channel to that measured at primary channel (see the channel number in Table I).

TABLE I. Definition of primary and secondary channel number for VNC2 and VNC3.

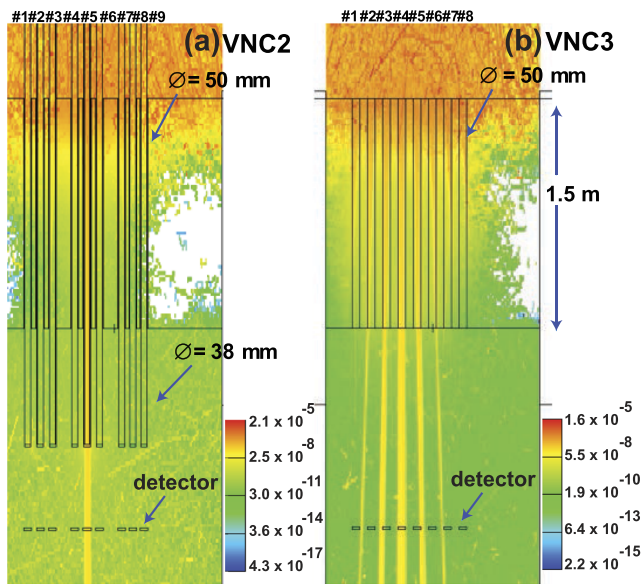|	Primary channel No.	Secondary channel No.
VNC2	#5 (R = 3.725 m)	#4 (R = 3.644 m) #6 (R = 3.806 m)
VNC3	#4 (R = 3.7 m)	#3 (R = 3.6 m) #5 (R = 3.8 m)

FIG. 4. Neutron flux distribution at the collimator and detector position of (a) VNC2 and (b) VNC3.

2. The VNC performance

Figure 5 shows the neutron spectra at the detector of primary channels of VNC2 and VNC3 in the energy range of 0.1 MeV –2.45 MeV. There are clear peaks of virgin neutron at an energy of 2.45 MeV, whereas the contribution of scattered neutron is continuous. The results show that the virgin neutron at the detector of VNC2 is about 54% lower than the virgin neutron at the detector of VNC3 due to smaller collimator diameter. The spectra show that neutron fluxes at the detector are dominated by over 99% of virgin 2.45 MeV neutrons. The spatial profiles of VNC2 and VNC3
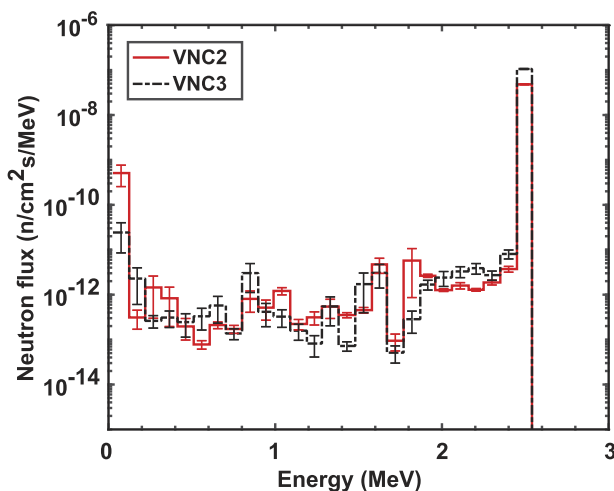

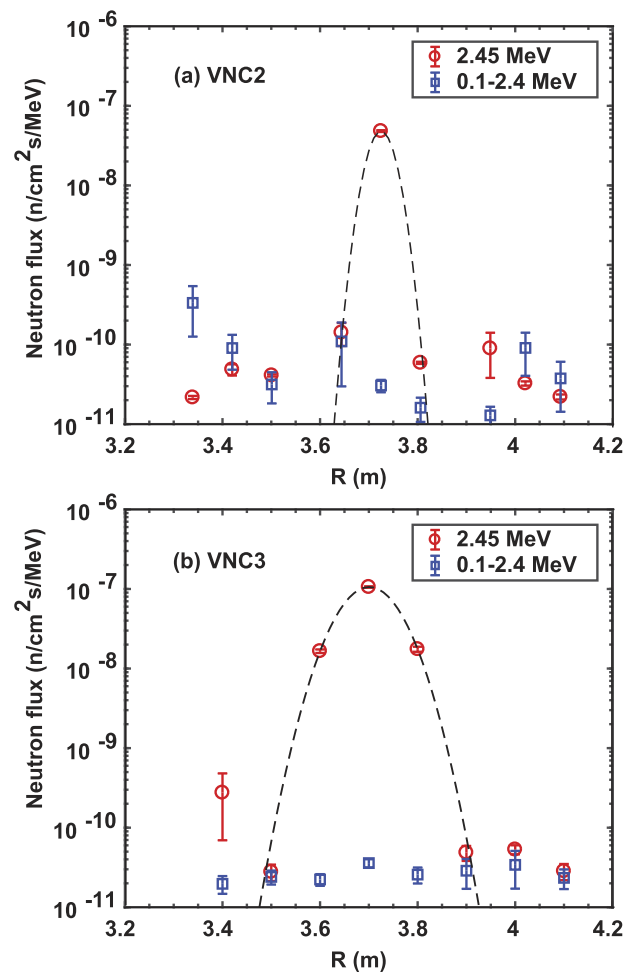**FIG. 5**. Neutron energy spectra at the primary channel's detector of VNC2 and VNC3.

FIG. 6. Neutron flux profiles of 2.45 MeV neutron and 0.1 MeV–2.4 MeV neutron at detector positions calculated for (a) VNC2 and (b) VNC3.

are conducted, as shown in Figs. 6(a) and 6(b). The scattered neutrons are approximately constant and approximately three orders of magnitude lower than the virgin 2.45 MeV neutrons on the primary channels. The neutron flux at the inner radius channel ($R = 3.339$ m of VNC2 and $R = 3.4$ m of VNC3) is about one order of magnitude higher than the neutron flux at the next channel due to the thin layer of heavy concrete in the inner radius side (see Fig. 3). Most of the neutron flux at the inner radius channel of VNC2 is dominated by scattered neutrons due to the collision in stainless steel pipes, while that at the inner radius channel of VNC3 is dominated by virgin neutrons streaming through the collimator.

The spatial resolutions have been estimated from the Gaussian fit of the 2.45 MeV neutron. It is found to be ~6 cm and ~13 cm in FWHM (Full Width at Half Maximum) for VNC2 and VNC3, respectively. The spatial resolution of VNC3 is about 5 cm wider than the spatial resolution that has been evaluated for VNC1[32] due to the broad distance between two sight lines and the larger collimator diameter. Furthermore, about 0.3% of neutron crosstalk is observed in VNC2, while about 16% is observed in VNC3 (see Table II).

TABLE II. Neutron crosstalk where Φ is total neutron flux.

	$\Phi_{primary}$	Average $\Phi_{secondary}$	Crosstalk
VNC2	4.8188×10^{-8}	1.6305×10^{-10}	0.0034
VNC3	1.0583×10^{-7}	1.7050×10^{-8}	0.1611

The obtained neutron crosstalk on VNC3 is high, which may cause the relatively high overestimation on the measured neutron flux. Therefore, the performance improvement toward the lower neutron crosstalk on VNC3 is determined. Discussion for reducing the neutron crosstalk is described in Sec. V.

IV. MEASUREMENT OF NEUTRON EMISSION PROFILE IN A P-NB HEATED PLASMA

Time-resolved measurement of the neutron emission profile was performed in the deuterium plasma experiment (Fig. 7). In this experiment, the magnetic axis position at vacuum R_{ax_vac} is set to be 3.6 m, toroidal magnetic field strength is set to be 2.75 T with clockwise (CW) direction from the top view, line average electron density n_{e_avg} of about 1.5×10^{19} m^{-3}, and central electron temperature T_{e0} of about 6 keV. The short pulses (~40 ms) P-NB#4, with an injection power of ~7 MW, have been injected into the electron cyclotron heated (ECH) plasma, with an ECH injection power of ~3 MW. Due to the short pulses P-NB, the S_n measured by the neutron flux monitor increases during the short pulse P-NB injection and decays after the P-NB stops. The line-integrated neutron emission profiles of averaged voltage in a function of R at t_1: 3.41 s–3.42 s, t_2: 3.43 s–3.44 s, and t_3: 3.45 s–3.46 s are analyzed and presented in Figs. 8(a) and 8(b). Line integrated neutron emission profiles measured by VNC2 has a peak at $R \sim 4.0$ m, whereas that measured by VNC3 has a peak at $R \sim 3.8$ m. Peaks of the obtained neutron emission profile are
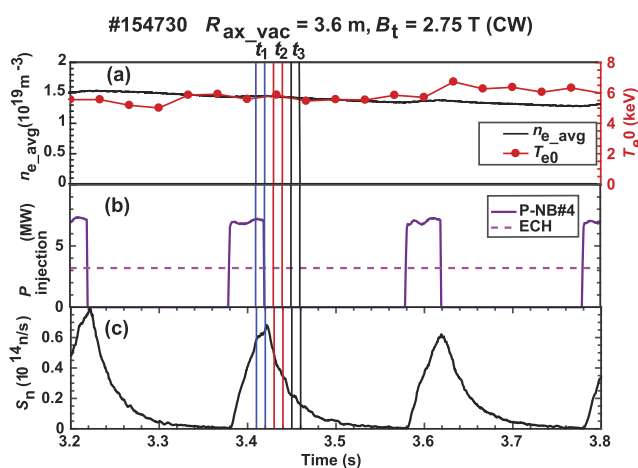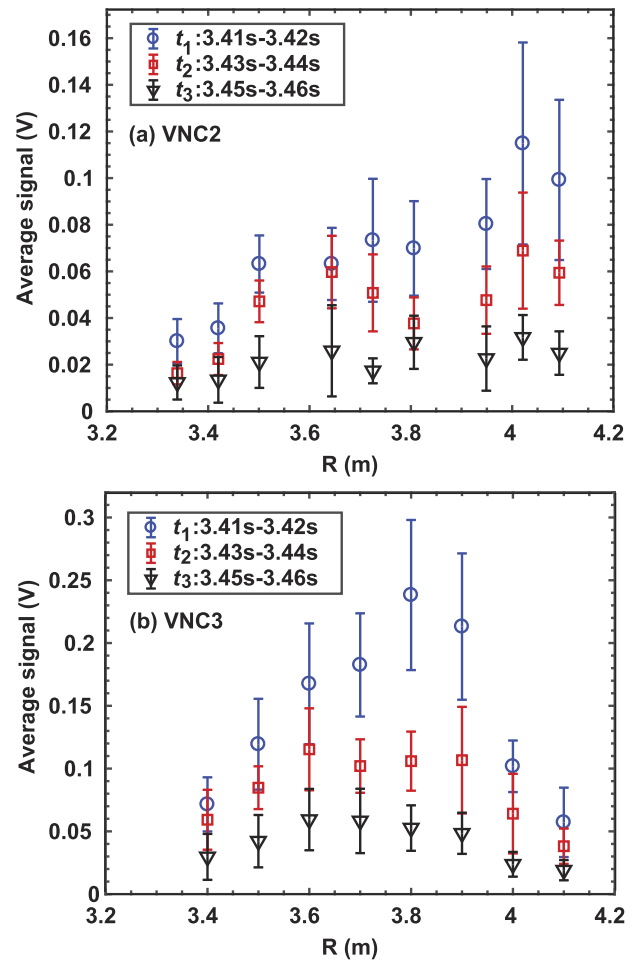

FIG. 8. The line-integrated neutron emission profile measured by (a) the VNC2 and (b) the VNC3.

consistent with the location of the helical ripple valley, as shown in Fig. 2. Moreover, it is clearly seen that the decrease in line integrated neutron flux at the peak positions after the beam stops is consistent with the S_n presented in Fig. 7(c). The results show that the neutron emission profile corresponding to the poloidal structure of helically trapped beam ion made by P-NB injection is successfully obtained.

V. VNC3 PERFORMANCE IMPROVEMENT TOWARD LOWER CROSSTALK

To reduce the neutron crosstalk, two conceptual designs, pre-collimator and leading pipe, have been introduced in the calculation model for VNC3. The pre-collimator is made of stainless steel (SS316L) with a 5 cm diameter cylinder hole on the same vertical axis of VNC3 and is placed above 1.5L port flange [Fig. 9(a)]. An array of stainless steel (SUS304) pipes with an inner diameter of 4.56 cm and an thickness of 0.15 cm are inserted vertically from 1.5L port along the VNC3 [Fig. 9(b)] as the leading pipe model. In this calculation, the pre-collimator thickness is varied between 5 cm and 30 cm,

FIG. 7. Time evolution of deuterium plasma shot No. 154730 performed at LHD. (a) Line-averaged electron density n_{e_avg} and central electron temperature T_{e0}. (b) The short pulses P-NB#4 and ECH are injected during selected time. (c) S_n measured by the LHD neutron flux monitor. Three time slices, t_1: 3.41 s–3.42 s, t_2: 3.43 s–3.44 s, and t_3: 3.45 s–3.46 s, are selected to determine the neutron emission profile.

FIG. 9. MCNP calculation model of VNC3 (a) pre-collimator and (b) leading pipe.

FIG. 10. Obtained results of neutron crosstalk and spatial resolution in FWHM for VNC3 with (a) different thicknesses of the pre-collimator and (b) different lengths of the leading pipe.

whereas the length of the leading pipe is varied between 50 cm and 465.2 cm (distance from 1.5L port to detector).

The neutron crosstalk is evaluated, and in addition, the spatial resolution is obtained. For the pre-collimator model [see Fig. 10(a)], the neutron crosstalk decreases exponentially, while the pre-collimator thickness increases. The number of total neutrons and virgin 2.45 MeV neutrons are almost the same, which means that the pre-collimator does not induce the scattered neutrons. Furthermore, the narrow FWHM is observed. The 15 cm thickness of the pre-collimator, with the weight of ~0.7 ton, provides less than 1% of the neutron crosstalk and a spatial resolution of ~6 cm in FWHM. It is found that at minimum, an FWHM of ~6 cm is limited by the distance between collimators. The obtained results show that pre-collimator can adjust to change the viewing cone of the sight line, resulting in the reduction of the neutron crosstalk and providing a better spatial resolution, while the direct neutron is not affected.

For the leading pipe model [see Fig. 10(b)], the short length leading pipes (between 50 cm and 120 cm in this study) provide the higher neutron crosstalk than the current VNC3 status due to the reduction of about 25% of the neutron flux in the primary channel but insignificant reduction of neutron flux in secondary channel. A steep decrease in the neutron crosstalk is obtained when the length of the leading pipe is more than 186 cm. The length more than 260 cm of leading pipes provides less than 1% of the neutron crosstalk and a spatial resolution of ~6.5 cm in FWHM. The obtained results show that appropriate length of leading pipe allows smaller collimator diameter and longer collimated neutron beam to the detector, resulting in the reduction of the neutron crosstalk and providing the better spatial resolution. On account of the engineering and interfacing constraints of LHD torus and VNC3, the leading pipe with the length of 465.2 cm and the total weight of 0.07 ton is considered and will be developed for VNC3 in order to provide the higher performance on the reduction of neutron crosstalk and higher spatial resolution of the neutron emission profile.
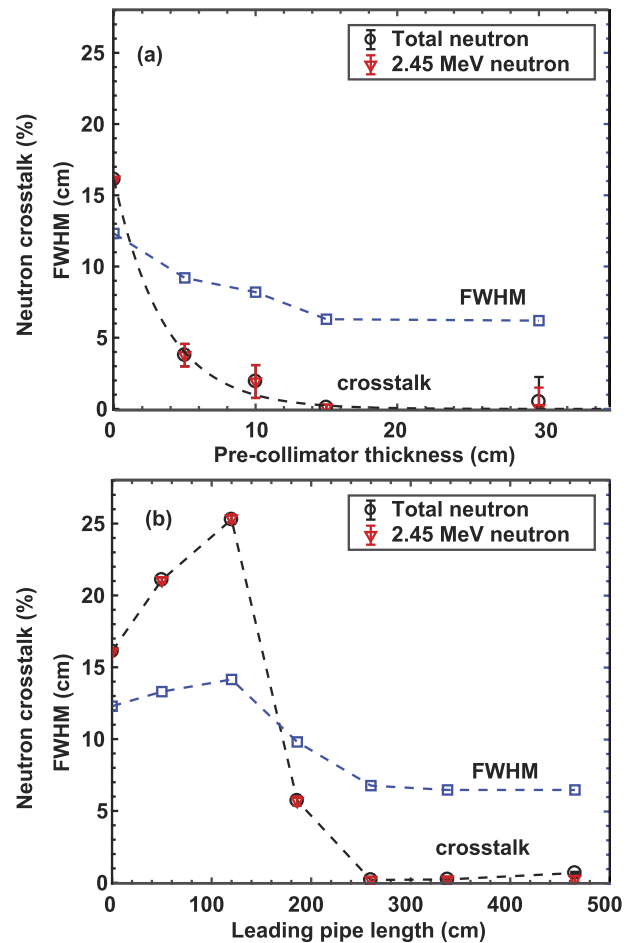
VI. SUMMARY

The performance of VNC2 and VNC3 at LHD has been evaluated using the MCNP6 calculation in this work. New vertical neutron cameras at LHD show the high collimation performance characterized by the high virgin neutron flux collimated to the detector. VNC2 provides a higher spatial resolution than VNC3 due to the additional 416 cm long stainless steel pipe along the collimator axis. The VNC2 and VNC3 show the capability to observe the poloidal structure of helically trapped beam ions created by the P-NBs injection at different plasma cross sections in the LHD deuterium experiment with the high temporal and spatial resolutions. In order to reduce the neutron crosstalk of VNC3, we are considering to install additional collimators, pre-collimator, and leading pipe. To achieve the 1% neutron crosstalk and design constraints, the leading pipe with 465.2 cm is suggested for installation on VNC3.

DATA AVAILABILITY

The data that support the findings of this study are available from the corresponding author upon reasonable request.

REFERENCES

[1] A. Fasoli, C. Gormenzano, H. L. Berk, B. Breizman, S. Briguglio, D. S. Darrow, N. Gorelenkov, W. W. Heidbrink, A. Jaun, S. V. Konovalov, R. Nazikian, J.-M. Noterdaeme, S. Sharapov, K. Shinohara, D. Testa, K. Tobita, Y. Todo, G. Vlad, and F. Zonca, "Chapter 5: Physics of energetic ions," Nucl. Fusion **47**, S264 (2007).

[2] A. L. Roquemore, R. C. Chouinard, M. Diesso, R. Palladino, J. D. Strachan, and G. D. Tait, "TFTR multichannel neutron collimator," Rev. Sci. Instrum. **61**, 3163 (1990).

[3] A. L. Roquemore, M. Bitter, L. C. Johnson, and S. von Goeler, "Recent expansion of the TFTR multichannel neutron collimator," Rev. Sci. Instrum. **68**, 544 (1997).

[4] J. M. Adams, O. N. Jarvis, G. J. Sadler, D. B. Syme, and N. Watkins, "The JET neutron emission profile monitor," Nucl. Instrum. Methods Phys. Res., Sect. A **329**, 277 (1993).

[5] O. N. Jarvis, J. M. Adams, F. B. Marcus, and G. J. Sadler, "Neutron profile measurements in the Joint European Torus," Fusion Eng. Des. **34-35**, 59–66 (1997).

[6] T. Craciunescu, G. Bonheure, V. Kiptily, A. Murari, S. Soare, I. Tiseanu, V. Zoita, and JET EFDA Contributors, "The maximum likelihood reconstruction method for JET neutron tomography," Nucl. Instrum. Methods Phys. Res., Sect. A **595**, 623 (2008).

[7] M. Ishikawa, T. Nishitani, A. Morioka, M. Takechi, K. Shinohara, M. Shimada, Y. Miura, M. Nagami, and Y. A. Kaschuck, "First measurement of neutron emission profile on JT-60U using stilbene neutron detector with neutron-gamma discrimination," Rev. Sci. Instrum. **73**, 4237 (2002).

[8] M. Ishikawa, T. Itoga, T. Okuji, M. Nakhostin, K. Shinohara, T. Hayashi, A. Sukegawa, M. Baba, and T. Nishitani, "Fast collimated neutron flux measurement using stilbene scintillator and flashy analog-to-digital converter in JT-60U," Rev. Sci. Instrum. **77**, 10E706 (2006).

[9] M. Ishikawa, M. Takechi, K. Shinohara, C. Z. Cheng, G. Matsunaga, Y. Kusama, A. Fukuyama, T. Nishitani, A. Morioka, M. Sasao, M. Baba, and JT-60 team, "Confinement degradation and transport of energetic ions due to Alfvén eigenmodes in JT-60U weak shear plasmas," Nucl. Fusion **47**, 849–855 (2007).

[10] F. B. Marcus, O. N. Jarvis, M. Loughlin, G. Sadler, P. Stott, J. M. Adams, D. S. Bond, N. P. Hawkes, N. Watkins, P. Batistoni, M. Rapisarda, T. Elevant, L. Johnson, L. de Kock, and C. Walker, "A neutron camera for ITER (Invited)," Rev. Sci. Instrum. **68**, 514 (1997).

[11] D. Marocco, B. Esposito, and F. Moro, "Neutron measurements in ITER using the radial neutron camera," J. Instrum. **7**, C03033 (2012).

[12] H. Matsushita, K. Ida, S. Okamura, M. Isobe, R. Akiyama, and Y. Yoshimura, "Loss cone boundary measurement using diagnostic neutral beam and neutral particle analyzer in a compact helical system," Rev. Sci. Instrum. **75**, 3607 (2004).

[13] M. Osakabe, M. Isobe, S. Murakami, S. Kobayashi, K. Saito, R. Kumazawa, T. Mutoh, T. Ozaki, M. Nishiura, E. Veshchev, T. Seki, Y. Takeiri, O. Kaneko, K. Nagaoka, T. Tokuzawa, K. Ogawa, K. Toi, S. Yamamoto, M. Sasao, T. Watanabe, and LHD Experiment Group, "Fast-ion confinement studies on LHD," Fusion Sci. Technol. **58**, 131–140 (2010).

[14] M. Isobe, M. Osakabe, T. Ozaki, M. Nishiura, P. V. Goncharov, E. Veshchev, K. Ogawa, K. Nagaoka, K. Saito, S. Murakami, T. Saida, M. Sasao, K. Toi, and LHD Experiment Group, "Fast-particle diagnostics on LHD," Fusion Sci. Technol. **58**, 426–435 (2010).

[15] T. Saida, M. Sasao, M. Isobe, A. V. Krasilnikov, R. Kumazawa, T. Mutoh, T. Watari, T. Seki, K. Saito, S. Murakami, K. Matsuoka, and LHD Experimental Group, "Study of ripple-trapped proton behaviour in LHD by two line-of-sight measurements of fast neutrals," Nucl. Fusion **44**, 488–495 (2004).

[16] M. Osakabe, Y. Takeiri, T. Morisaki et al., "Current status of Large Helical Device and its prospect for deuterium experiment," Fusion Sci. Technol. **72**, 199–210 (2017).

[17] M. Isobe, K. Ogawa, T. Nishitani, N. Pu, H. Kawase, R. Seki, H. Nuga, E. Takada, S. Murakami, Y. Suzuki, M. Yokoyama, M. Osakabe, and LHD Experiment Group, "Fusion neutron production with deuterium neutral beam injection and enhancement of energetic-particle physics study in the Large Helical Device," Nucl. Fusion **58**, 082004 (2018).

[18] K. Ogawa, M. Isobe, T. Nishitani, S. Murakami, R. Seki, H. Nuga, S. Kamio, Y. Fujiwara, H. Yamaguchi, Y. Saito, S. Maeta, M. Osakabe, and LHD Experiment Group, "Energetic ion confinement studies using comprehensive neutron diagnostics in the Large Helical Device," Nucl. Fusion **59**, 076017 (2019).

[19] M. Isobe, K. Ogawa, T. Nishitani, H. Miyake, T. Kobuchi, N. Pu, H. Kawase, E. Takada, T. Tanaka, S. Li, S. Yoshihashi, A. Uritani, J. Jo, S. Murakami, M. Osakabe, and LHD Experiment Group, "Neutron diagnostics in the Large Helical Device," IEEE Trans. Plasma Sci. **46**, 2050–2058 (2018).

[20] K. Ogawa, M. Isobe, E. Takada, Y. Uchida, K. Ochiai, H. Tomita, A. Uritani, T. Kobuchi, and Y. Takeiri, "Progress in development of the neutron profile monitor for the Large Helical Device," Rev. Sci. Instrum. **85**, 11E110 (2014).

[21] K. Ogawa, M. Isobe, T. Nishitani, and T. Kobuchi, "The Large Helical Device vertical neutron camera operating in the MHz counting rate range," Rev. Sci. Instrum. **89**, 113509 (2018).

[22] K. Ogawa, M. Isobe, H. Kawase, T. Nishitani, R. Seki, M. Osakabe, and LHD Experiment Group, "Observation of enhanced radial transport of energetic ion due to energetic particle mode destabilized by helically-trapped energetic ion in the Large Helical Device," Nucl. Fusion **58**, 044001 (2018).

[23] K. Ogawa, M. Isobe, H. Kawase, T. Nishitani, R. Seki, M. Osakabe, and LHD Experiment Group, "Effect of the helically-trapped energetic-ion-driven resistive interchange modes on energetic ion confinement in the Large Helical Device," Plasma Phys. Controlled Fusion **60**, 044005 (2018).

[24] S. Murakami, A. Wakasa, H. Maaberg, C. D. Beidler, H. Yamada, K. Y. Watanabe, and LHD Experimental Group, "Neoclassical transport optimization of LHD," Nucl. Fusion **42**, L19 (2002).

[25] R. Seki, Y. Matsumoto, Y. Suzuki, K. Watanabe, K. Hamamatsu, and M. Itagaki, "Monte-Carlo study based on real coordinates for perpendicularly injected high-energy ions in the LHD high-beta plasma," Plasma Fusion Res. **5**, 014 (2010).

[26] See https://eljentechnology.com/images/products/data_sheets/EJ-410.pdf for the specification of EJ-410.

[27] See https://www.hamamatsu.com/resources/pdf/etd/High_energy_PMT_TPMZ0003E.pdf for the specification of H7195 PMT.

[28] See https://s1.dtsheet.com/store/data/000749671.pdf?key=2f4cb749296cb6e8895ac79f7a1c378a&r=1 for the specification of C7319 preamplifier unit.

[29] See https://www.ni.com/pdf/manuals/371231d.pdf for the specification of fast digitizer acquisition system PXI6133.

[30] D. B. Pelowits, MCNP6 User's Manual, LA-CP-13-00634, Los Alamos National Laboratory, 2013, https://mcnp.lanl.gov/mcnp_manual.shtml.

[31] M. B. Chadwick et al., "ENDF/B-VII. 1 nuclear data for science and technology: Cross sections, covariances, fission product yields and decay data," Nucl. Data Sheets **112**, 2887–2996 (2011).

[32] T. Nishitani, K. Ogawa, and M. Isobe, "Monte Carlo simulation of the neutron measurement for the Large Helical Device deuterium experiments," Fusion Eng. Des. **123**, 1020–1024 (2017).

[33] H. Kawase, K. Ogawa, T. Nishitani, N. Pu, M. Isobe, and LHD Experiment Group, "Evaluation of spatial resolution of neutron profile monitor in LHD," IEEE Trans. Plasma Sci. **47**, 462–465 (2019).

[34]T. Nishitani, K. Ogawa, H. Kawase, N. Pu, T. Ozaki, and M. Isobe, "Monte Carlo calculation of the neutron and gamma-ray distributions inside the LHD experimental building and shielding design for diagnostics," Prog. Nucl. Sci. Technol. **6**, 48–51 (2019).

[35]T. Nishitani, K. Ogawa, K. Nishimura, and M. Isobe, "Radiation field estimation for the diagnostic and control components by Monte Carlo neutronics calculations with LHD 3-dimensional modeling," Plasma Fusion Res. **11**, 2405057 (2016).

[36]S. Kamio, Y. Fujiwara, K. Ogawa, M. Isobe, R. Seki, H. Nuga, T. Nishitani, M. Osakabe, and LHD Experiment Group, "Development of NPA array using single crystal CVD diamond detectors," J. Instrum. **14**, C08002 (2019).